Phys 7123 Final Project.

Quasihorizontal Chaotic Mixing in Reanalysis Windfields

Jonathon Wright

Georgia Institute of Technology, Atlanta, GA

Abstract. One of the prevailing hindrances to the development of more accurate climate models is the current inability to correctly model transport and diffusion of chemical tracers in the atmosphere. Outfitting the model with accurate mixing parameterizations becomes too computationally expensive, yet neglecting these effects yields physically unrealistic output. We analyze transport and diffusion on an annual scale by calculating Lyapunov exponents, drift and diffusion in European Centre for Medium-Range Weather Forecasting (ECMWF) ERA-15 reanalyses of global 315 K isentropic windfields. We present a Lagrangian model of isentropic chaotic mixing for use in more expansive future studies.

1. Introduction

Chaotc mixing is widely recognized as a major factor in determining the distribution of chemical tracers and aerosols in the atmosphere, yet scientific understanding of the processes involved remains limited. We have developed a model of isentropic chaotic mixing in the atmosphere following the general approach of *Pierrehumbert and Yang* (1993, herafter PY93). As in PY93, we have performed our analysis on the 315 K isentropic surface, since it generally does not intersect either the ground or the tropopause. On average, this surface is located at approximately 300 hPa at the poles and dips to around 600 hPa in the tropics. Since trajectories are evaluated along isentropic surfaces, each parcel should be seen as adiabatically contracting and expanding as necessary along its path. As in PY93, we have neglected diabatic motions across the isentropic surface.

While PY93 has served as the basis for this work, our analysis differs in significant ways. Whereas PY93 used once-daily windfields from a global general circulation model (GCM) to drive global Lyapunov exponents, we will use 4-times-daily reanalysis windfields from the European Centre for Medium-Range Weather Forecasting (ECMWF) ERA-15 dataset, which were unavailable when PY93 was published. In addition, while all integrations presented in PY93 were run for only 60 days beginning on January 1 of the GCM model run, we provide results for the complete annual solar cycle. Most significantly, however, we have chosen to evaluate Lyapunov exponents using a trajectory separation method rather than the matrix formulation presented in PY93. In future work, we will compare the two methods in terms of both proximity of results and computational expense.

We have chosen here to calculate Lyapunov exponents and drift as measures of predictability, along with diffusion as an indicator of the maximal rate of spread we would likely observe in passive tracer fields that originate at a given location. In future studies, we will examine how variability in these fields may relate to large-scale atmospheric events, such as fluctuations in the El Niño - Southern Oscillation (ENSO), North Atlantic Oscillation (NAO), and solar cycle, and the eruption of Mount Pinatubo in 1991.

The model presented here is essentially functional, although modifications still need to be made on the current methods and parameterizations. The results should be viewed as preliminary, and have not been extensively tested or independently verified. This remains a work in progress, but will serve as the basis for more extensive future studies.

2. Data

ECMWF ERA-15 reanalyses of geopotential height are used to determine the isentropic windfield for

integration with the trajectory advection model described below. ERA-15 was the initial product of the ECMWF reanalysis project, which intends to improve studies of climate by providing consistent meteorological data over long time scales. The data assimilation scheme used by ERA-15 remains invariant throughout the 15 year reanalysis period to be used in this study..

Spurious fluctuations in tropical temperatures have been noted in these reanalyses on several timescales [*Trenberth et al.*, 2001]. These discrepancies should not adversely affect this study, but will be considered in the future as we analyze the results in terms of large-scale atmospheric circulations.

We use the method of *Randel* (1992) to derive temperatures, potential temperatures, and horizontal velocities from ERA-15 geopotential heights. Temperature T is evaluated via the hydrostatic relation, where we have assumed dry air for simplicity:

$$T = -\frac{g}{R}\frac{\partial \mathrm{Z}}{\partial \ln p} \tag{1}$$

where Z is the ERA-15 geopotential height, $\ln p$ is the logarithm of the associated pressure level, g is the gravitational constant ($9.81 ms^{-2}$), and R is the gas constant for dry air ($287 m^2 s^{-2} K^{-1}$).

Potential temperature θ is then calculated as:

$$\theta = T\left(\frac{1013\mathrm{mb}}{p}\right)^{\kappa} \tag{2}$$

where 1013 mb represents average sea level pressure and $\kappa = 2/7$.

Zonal mean winds outside the tropics are determined using the gradient wind expression:

$$\frac{\bar{u}^2}{a}\tan\phi + 2\Omega\sin\phi\cdot\bar{u} + \frac{g}{a}\frac{\partial \bar{\mathrm{Z}}}{\partial\phi} = 0 \tag{3a}$$

while values in the tropical band from $\pm 10^\circ$ latitude are linearly interpolated from the values at $\pm 12.5^\circ$. Zonal Fourier components of the horizontal winds are derived from the zonal and meridional momentum equations linearized about the zonal mean wind:

$$\frac{\bar{u}}{a\cos\phi}\frac{\partial u'}{\partial\lambda} + \hat{f}v' + \frac{g}{a\cos\phi}\frac{\partial \mathrm{Z}'}{\partial\lambda} = 0, \tag{3b}$$

$$\frac{\bar{u}}{a\cos\phi}\frac{\partial v'}{\partial\lambda} + \tilde{f}u' + \frac{g}{a}\frac{\partial \mathrm{Z}'}{\partial\phi} = 0. \tag{3c}$$

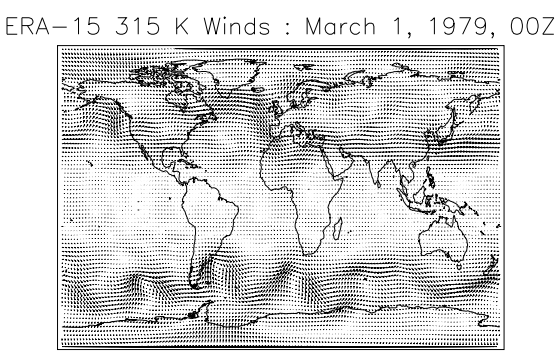

Figure 1. An example of the windfield produced using the data import and interpolation procedure described in Section 3.

In equations (3a-c), λ denotes longitude, ϕ latitude, a the radius of the earth (6.37×106 m), Ω the rotation rate of the earth (7.3×106 m), and u and v the zonal and meridional velocity components, respectively. Zonal means are represented by overbars, deviations by primes, and

$$\hat{f} = \left[2\Omega\sin\phi - \frac{1}{a\cos\phi}\frac{\partial}{\partial\phi}(\bar{u}\cos\phi)\right], \tag{4a}$$

$$\tilde{f} = \left[2\Omega\sin\phi + \frac{2\bar{u}}{a}\tan\phi\right]. \tag{4b}$$

Equations 3b-c are solved for each zonal wave number to determine the spectral coefficients of u' and v'. Since these equations become singular in zonal wavenumber k as

$$\delta \equiv \frac{(\bar{u}\cdot k/a\cos\phi)2}{\hat{f}\tilde{f}} \to 1, \tag{5}$$

we substitute the geostrophic winds

$$v_g = \frac{g}{2\Omega\sin\phi}\frac{\partial \mathrm{Z}}{\partial x},\ u_g = \frac{g}{2\Omega\sin\phi}\frac{\partial \mathrm{Z}}{\partial y} \tag{6}$$

if $\delta > 0.5$.

Pressure, temperature, and wind are then linearly interpolated onto surfaces of constant θ to allow for an analysis of quasi-horizontal mixing on isentropic

surfaces. The windfield for March 1, 1979 on the 315 K isentropic surface determined using this method is shown in Figure 1. A qualitative comparison with the composite mean vector wind for this same day using NCEP/NCAR reanalyses (not shown) indicates a very good measure of agreement.

3. Governing Equations and Model Formulation

This project centers around the determination of attributes of quasi-horizontal motion along an isentropic surface in the atmosphere. We initialize the quasi-horizontal windfield $[u(x, y, t), v(x, y, t)]$ using the ECMWF ERA-15 reanalyses of geopotential height to project the velocity field onto the 315 K potential temperature surface as described above. For purposes of this discussion, we will consider this surface to be a horizontal Cartesian plane with coordinates $[x, y]$.

Given the velocity field, the trajectory evolution of a specified grid point is evaluated using a Runge-Kutta fourth order numerical integration with one hour time steps on the following ordinary differential equations:

$$\frac{dx}{dt} = u(x, y, t), \ \frac{dy}{dt} = v(x, y, t) \tag{7}$$

subject to initial conditions $[x(0), y(0)] = (x_0, y_0)$. We evaluate an ensemble of such trajectories, where each corresponds to an initial condition defined by the $2.5^\circ \times 2.5^\circ$ grid.

While the velocity data is archived using a gridded cylindrical equidistant projection of the globe, we normalize distance along the surface of the earth ellipsoid by iterating Vincenty's direct and inverse formulae, outlined in the Appendix [*Vincenty*, 1975]. This method allows for a considerable measure of flexibility in accuracy and computational speed. While we have opted here for speed at the expense of accuracy, the code can be easily adapted for use in future work. Accuracy in our implementation remains within a few hundredths of a degree.

We have chosen to present this analysis in terms of three aspects of the annual circulation: Lyapunov exponents, drift, and diffusion. Lyapunov exponents provide a lower bound on the predictability of trajectories originating at a given gridpoint, drift provides a more accurate measure of mixing characteristics and predictability, and diffusion represents a measure of the rate of spread for a passive tracer released at a given gridpoint. All three quantities are computed using a trajectory spreading algorithm.

Each gridpoint is initialized with a neighbor, in this case the immediately neighboring gridpoint to the south. The two trajectories are integrated until the separation grows to a pre-determined factor of the initial separation (We present the results of integrations using factors of 5 and 10 in Section 4). When this distance is exceeded, the focus point remains where it is, and the neighbor is reset to a unit distance away on the grid in the same direction as it finished. The process is iterated until the parcel has undergone a complete annual cycle.

Average annual Lyapunov exponents are calculated using the formula:

$$\lambda = \frac{1}{T} \sum_i \frac{1}{t_i} \ln \left| \frac{\Delta x(t_i)}{\Delta x(0)} \right| \tag{8}$$

where i represents each segment in which the separation between the gridpoint in question and its neighbor grows to exceed the chosen factor, t_i is the time required for that separation to be realized, and $\Delta x(0)$ and $\Delta x(t_i)$ are the initial and final separations, respectively. T denotes the number of segments i that take place over the course of the year. It should be noted that $\Delta x(0)$ may vary from segment to segment due to position on the globe or direction between neighboring points.

Drift is determined similarly:

$$\tilde{v} = \frac{1}{T} \ln \left| \sum_i \frac{1}{t_i} \frac{\Delta x(t_i)}{\Delta x(0)} \right| \tag{9}$$

This formulation should provide a more accurate measure of predictability in the system than the Lyapunov exponent, since the calculation retains directional considerations during the summation, rather than relying solely on distance. Note that the Lyapunov exponent provides an upper bound on this quantity.

We also calculate diffusion as a measure of the rate of spread using the time-averaged square of the difference between final distance and initial distance:

$$\mathrm{D} = \frac{1}{T} \sum_i < (x(t_i) - x(0))^2 > \tag{10}$$

where <> denotes the time average, and all other notation remains as in equation 8.

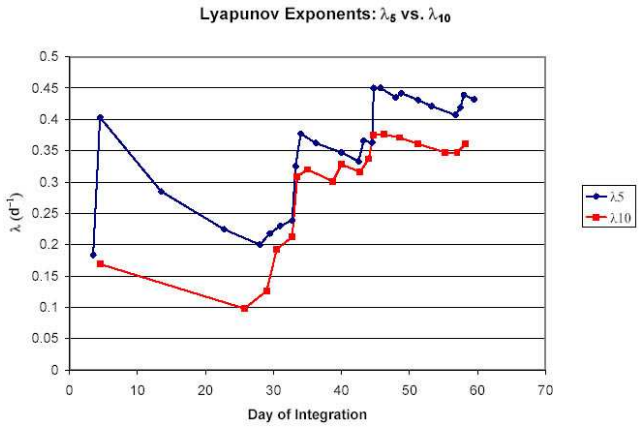

Figure 2. Lyapunov exponents for the trajectory starting at 32.5° N and 275° E and running for 60 days from January 1, 1979. λ_5 is shown in blue and λ_{10} in red.

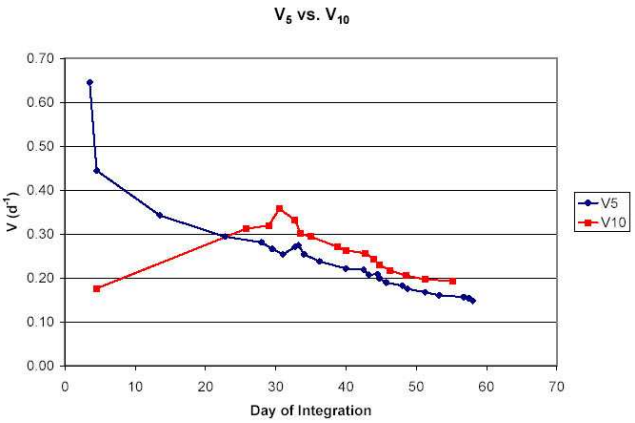

Figure 3. As in Figure 2 but for drift [d^{-1}].

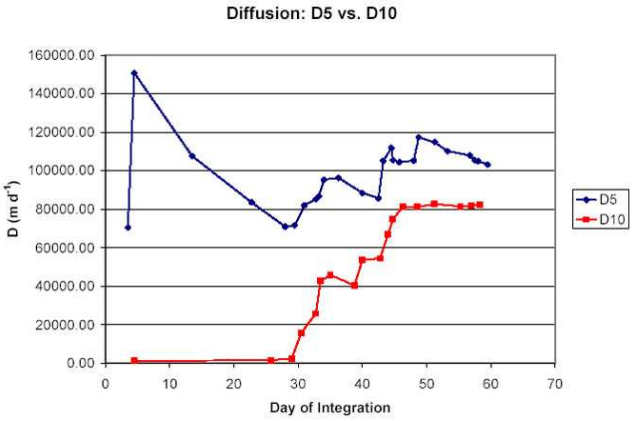

Figure 4. As in Figure 2 but for diffusion [m d^{-1}].

4. Results

We have calculated the evolution of all three quantities for the trajectory starting at 32.5° N and 275° E, near Atlanta, Georgia, United States. This integration begins on January 1, 1979 and continues for 60 days. Initial results indicate that the values of the Lyapunov exponents calculated are somewhat dependent upon the choice of separation factor, although the trends appear similar [Figure 2].

In this case, we have used a separation threshold factor of 5 and compared it to a factor of 10. At 4.5 days into the integration, $lambda_5 = .403$ d^{-1}, while $lambda_{10} = .169$ d^{-1}. By day 40, however, the difference between $lambda_5$ and $lambda_{10}$ is only .019 d^{-1}. At the end of 60 days, $lambda_5$ has spiked to .432 d^{-1}, while $lambda_{10}$ has plateaued at around .361 d^{-1}. For purposes of comparison, afterthe full year of integration, $lambda_5 = .394$ d^{-1}, while $lambda_{10} = .295$ d^{-1}. Both values are within the range of Lyapunov exponents reported by PY93.

We retain a measure of uncertainty about the validity of our results for drift and diffusion (Figure 3a, b), but are confident that this can be resolved in the near future. Initial results indicate that the value for $\tilde{v}$ for trajectories originating at 32.5° N and 275° E and running for 365 days is approximately 0.04 d^{-1}, while D appears to be between 5.5 and 6.5×10^4 m d^{-1}. Drift decreases monotonically with length of integration, which may require us to revise our formula, and we have not yet devised a way to independently verify diffusion. We will use extensive model runs that cover the 15 year period to help evaluate these results, in addition to consulting additional sources and possibly refining our methods.

Figure 4 shows the global distribution for all three quantities after the yearlong run of wind data from 1979. The distributions are more homogeneous than we expected based on PY93. It should be remembered, however, that PY93 ran the model for only 60 days. Since the transport timescale between hemispheres is usually around 6 months and within the hemispheres is much shorter, the length of integration may allow the majority of trajectories to converge to a few large-scale convergence zones that then dominate the results. In the future, we will generate global maps every 30 days into the integration to better describe the evolution of the Lyapunov exponent, drift, and diffusion fields.

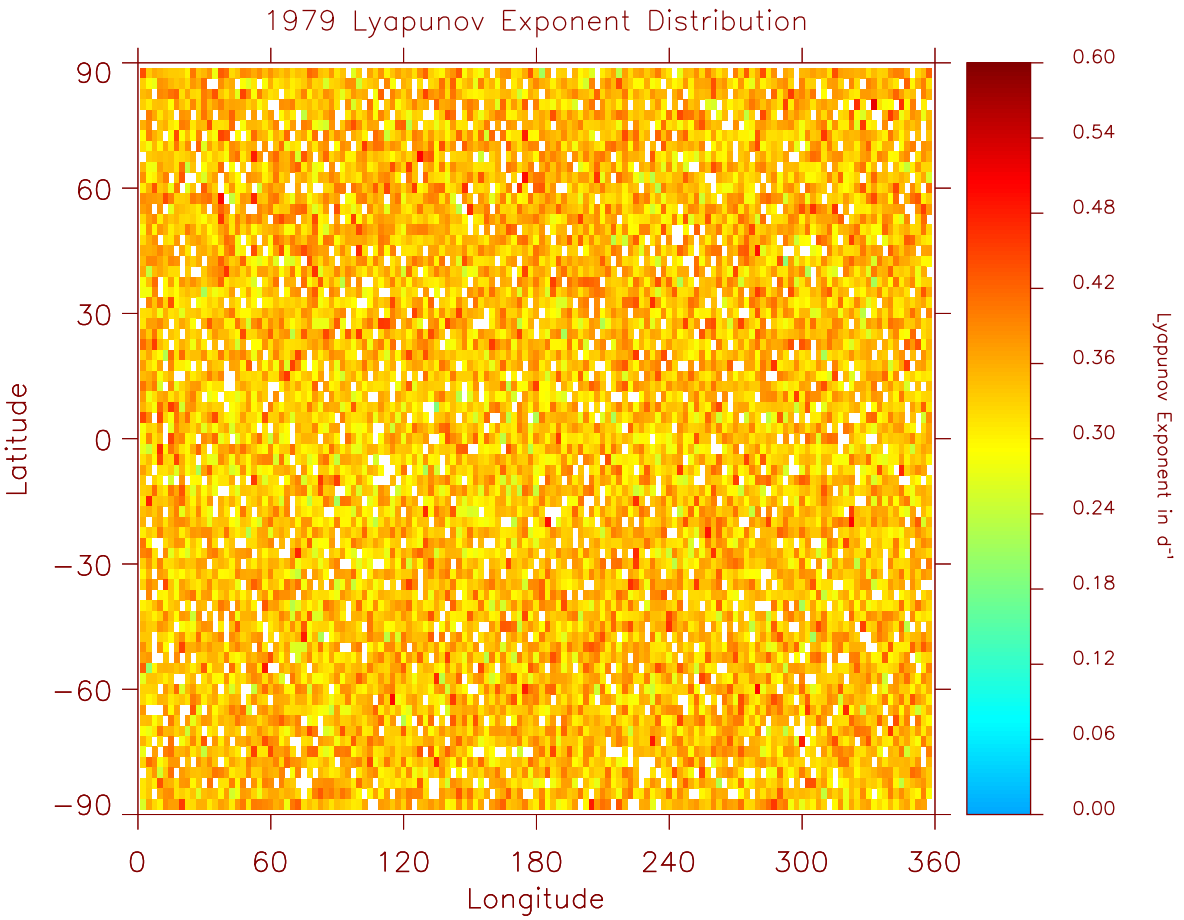

(a) Lyapunov Exponents

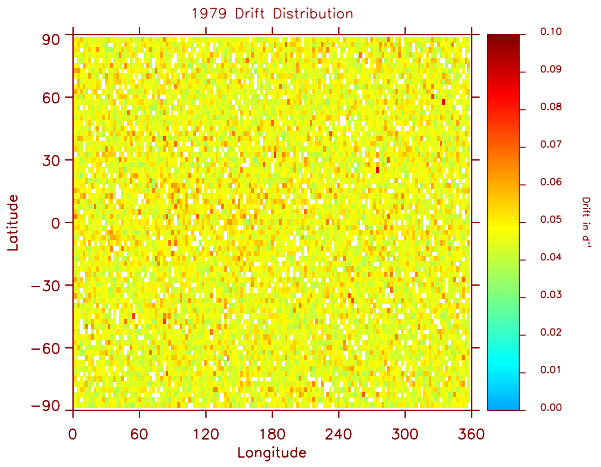

(b) Drift

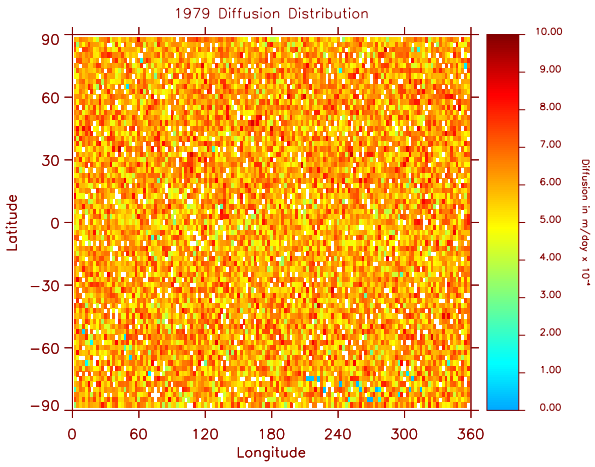

(c) Diffusion

Figure 5. (a) Lyapunov exponent, (b) drift, and (c) diffusion distributions for the full 365 day integration of 1979. The distributions appear to be relatively homogeneous, which may be caused by the majority of trajectories being attracted by areas of convergence that dominate the results. We will generate output for shorter timescales as well in an effort to determine when this homogeneity sets in.

5. Discussion and Future Work

We have presented a method for calculating Lyapunov exponents, drift, and diffusion from isentropic windfields that can serve as the basis for intensive studies of atmospheric mixing and climate variability. While much remains to be done, initial results appear to be within reasonable ranges.

We will extend the preliminary findings presented here to encompass the entire 15-year climatology, and we will proceed as planned with our analysis of relationships between changes in the Lyapunov exponents, drift, and diffusion, and large-scale atmospheric variability. We will also attempt to implement the matrix formulation method for determing Lyapunov exponents detailed in PY93 and compare the results to those obtained using the trajectory separation method described in Section 3. We will likely supplement these studies by tracking the evolution of various initial distributions of passive tracer within the model and investigating sensitivity in the model by performing the calculations with different levels of accuracy.

While this project has been limited by time constraints, now that the base model is complete, we will consider the utility of additional datasets (such as the 40-year ECMWF reanalysis product or the NCEP reanalyses), as well as the potential of examining regional variability at smaller time and spatial scales using satellite retrievals.

The potential applications of the methods described here are not limited to the questions discussed. In particular, this method could be used to explore whether the atmospheric circulation is recurrent on long timescales or not. This investigation could eventually lead to attempts to detect and classify recurrent motions in the atmosphere, which could in turn have strong implications for climate change prediction.

Appendix A: Appendix: Vincenty's Formulae

The notation in the following description of Vincenty's formulae follows that given in *Vincenty* [1975]. A more complete explanation of the equations and the associated error can be found in that reference.

A1. Direct Formula

The point on a sphere a certain distance s and azimuthal direction α_1 away from a given point P_1 is calculated by first computing

$$\tan\sigma_1 = \tan(U_1/\cos\alpha_1), \tag{A1a}$$

$$\sin\alpha = \cos U_1 \sin\alpha, \tag{A1b}$$

$$A = 1 + \frac{u^2}{256}[64 + u^2(-12 + 5u^2)], \tag{A1c}$$

and

$$B = \frac{u^2}{512}[128 + u^2(-64 + 37u^2)]. \tag{A1d}$$

where U_1 is given by

$$\tan U_1 = (1 - f)\tan\phi_1, \tag{A2}$$

f is the flattening factor given by $(a-b)/a$, σ_1 is the angular distance on the sphere from the equator to P_1, α is the directional azimuth at the equator, and

$$u^2 = \cos^2\alpha(a^2 - b^2)/b^2 \tag{A3}$$

where a and b are the major and minor semiaxes of the earth, 6378 km and 6357 km, respectively. Then the following set of equations are iterated until the change in angular distance σ between P_1 and P_2 is negligible:

$$2\sigma_m = 2\sigma_1 + \sigma \tag{A4a}$$

$$\Delta\sigma = B\sin\sigma[\cos 2\sigma_m + \frac{1}{4}B\cos\sigma(-1 + 2cos^2 2\sigma_m)] \tag{A4b}$$

$$\sigma = \frac{s}{bA} + \Delta\sigma. \tag{A4c}$$

where σ_m is the angular distance on the sphere from the equator to the midpoint of the line between P_1 and P_2. The computation is then finished by calculating

$$\gamma = \sqrt{\sin^2\alpha + (\sin U_1 \sin\sigma - \cos U_1 \cos\sigma \cos\alpha_1)^2} \tag{A5a}$$

$$\tan\phi_2 = \frac{\sin U_1 \cos\sigma + \cos U_1 \sin\sigma \cos\alpha_1}{(1-f)\gamma} \quad \text{(A5b)}$$

$$\tan\lambda = \frac{\sin\sigma \sin\alpha_1}{\cos U_1 \cos\sigma - \sin U_1 \sin\sigma \cos\alpha_1} \quad \text{(A5c)}$$

$$C = \frac{f}{16}\cos^2\alpha[4 + f(4 - 3\cos^2\alpha)] \quad \text{(A5d)}$$

$$\beta = \sin\sigma[\cos 2\sigma_m + C\cos\sigma(-1 + 2\cos^2 2\sigma_m)] \quad \text{(A5e)}$$

$$L = \lambda - (1-C)f\sin\alpha[\sigma + C\beta] \quad \text{(A5f)}$$

where λ is the difference in longitude on an auxiliary sphere, ϕ_2 is the latitude of P_2, and L is the difference in longitude between P_1 and P_2.

A2. Inverse Method

The distance between two points on a sphere is determined using a first approximation of $\lambda = L$ and then iterating until the change in λ is negligible.

$$\sin^2\sigma = (\cos U_2 \sin\lambda)^2 + (\cos U_1 \sin U_2 - \sin U_1 \cos U_2 \cos\lambda)^2 \quad \text{(A6a)}$$

$$\cos\sigma = \sin U_1 \sin U_2 + \cos U_1 \cos U_2 \cos\lambda \quad \text{(A6b)}$$

$$\tan\sigma = \sin\sigma / \cos\sigma \quad \text{(A6c)}$$

$$\sin\alpha = \cos U_1 \cos U_2 \sin\lambda / \sin\sigma \quad \text{(A6d)}$$

$$\cos 2\sigma_m = \cos\sigma - 2\sin U_1 \sin U_2 / \cos^2\alpha \quad \text{(A6e)}$$

where U_2 is calculated as in equation 2. The calculation is then finished with

$$s = bA(\sigma - \Delta\sigma) \quad \text{(A7)}$$

where $\Delta\sigma$ is calculated from equations (A1c), (A1d), and (A3b).

Acknowledgments. We are grateful to P. Cvitanović for helpful suggestions.

References

Pierrehumbert, R. T., and H. Yang, Global chaotic mixing on isentropic surfaces, *J. Atmos. Sci., 50,* 2462-2480, 1993.

Randel, W. J., Global atmospheric circulation statistics, 1000-1 mbar, NCAR Tech. Note NCAR/TN-366+STR, NCAR, Boulder CO, 1992.

Trenberth, K. E., D. P. Stepaniak, and J. W. Hurrell, Quality of reanalysesin the tropics, *J. Clim., 14*, 1499-1510, 2001.

Vincenty, T., Direct and inverse solutions of geodesics on the ellipsoid with application of nested equations, *Survey Review, 176*, 88-93, 1975.

J. Wright, School of Earth and Atmospheric Sciences, Georgia Institute of Technology, Atlanta, GA 30332. (email: jswright@eas.gatech.edu)

This preprint was prepared with AGU's LaTeX macros v5.01. File 7123proposal3 formatted December 12, 2003.

With the extension option 'AGU^{++}' v1.0b.